The Journal of Supercritical Fluids 216 (2025) 106452

Contents lists available at ScienceDirect

The Journal of Supercritical Fluids

journal homepage: www.elsevier.com/locate/supflu

Supercritical CO_2 assisted bioMOF drug encapsulation and functionalization for delivery with a synergetic therapeutic value

Albert Rosado [a,*], Luis García-Fernández [b,c], María Rosa Aguilar [b,c], Rosa Ana Ramírez [b,c], Ana M. López-Periago [a], José A. Ayllón [d,*], Concepción Domingo [a,*]

[a] Materials Science Institute of Barcelona (ICMAB-CSIC), Campus UAB s/n, Bellaterra 08193, Spain
[b] Instituto de Ciencia y Tecnología de Polímeros (ICTP-CSIC), C/Juan de la Cierva, 3, Madrid 28006, Spain
[c] Networking Biomedical Research Centre in Bioengineering, Biomaterials and Nanomedicine (CIBER-BBN), Av. Monforte de Lemos, 3-5, Madrid 28029, Spain
[d] Departament de Química, Universitat Autònoma de Barcelona (UAB), Campus UAB s/n, Bellaterra 08193, Spain

HIGHLIGHTS

- CaSyr-1 bioMOF is processed *via* $scCO_2$ to afford a novel drug delivery system.
- $ScCO_2$ enables consecutive isoniazid impregnation and stearate functionalization.
- The followed green processing approach results in a system with null cytotoxicity.
- The assembled CaSyr-1(INH)/S/PS60 promotes sustained release of bioactive entities.

GRAPHICAL ABSTRACT

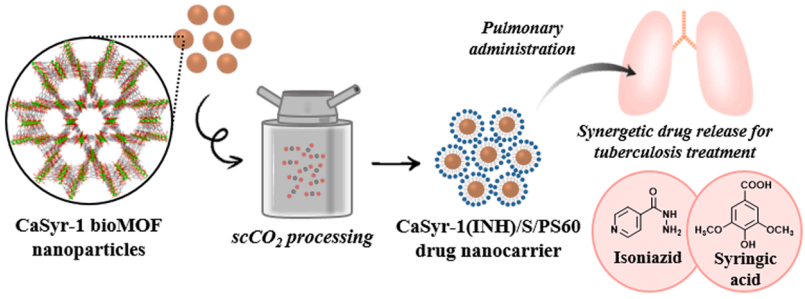

ARTICLE INFO

Keywords:
BioMOF
Supercritical CO2 processing
Hydrophobic functionalization
Stearic acid
Drug delivery

ABSTRACT

Despite the impressive characteristics of biological metal organic frameworks (bioMOFs) for their use as drug delivery systems (DDs), there are still some parameters related to their structural stability and processing routes that have decelerated their realistic application in this field. Both drawbacks are unraveled in this work for the microporous bioMOF CaSyr-1 by using supercritical CO_2 ($scCO_2$) to load the bioMOF with the anti-tubercular isoniazid (INH) drug, and functionalize its external surface with a hydrophobic protective layer of stearate (S). The hydrophobicized CaSyr-1(INH)/S vehicle is further coated with a neutral surfactant (PS60) to enhance the wettability of the system. *In vitro* tests, related to drug carrier biocompatibility and drug release in body simulated fluids, are performed to demonstrate potential prospective of the designed DDs in pharmacy. The synthetized product displayed total biocompatibility even at high concentrations, and the particle size and dissolution rate showed to be adequate for pulmonary administration.

* Corresponding authors.
E-mail addresses: arosado@icmab.es (A. Rosado), JoseAntonio.Ayllon@uab.es (J.A. Ayllón), conchi@icmab.es (C. Domingo).

https://doi.org/10.1016/j.supflu.2024.106452
Received 7 August 2024; Received in revised form 4 November 2024; Accepted 4 November 2024
Available online 5 November 2024

1. Introduction

Controlled and intelligent drug delivery systems (DDs) are of enormous interest for simultaneously maximizing active agents therapeutic efficacy and minimizing side effects [1]. These technological systems were first designed for the delivery of small drug molecules with a release largely dictated by their physicochemical properties, thus enabling entirely new medical treatments by sustaining the release, broadening the activity, increasing systemic circulation, adjusting the pharmacokinetics/bioavailability or enhancing the target to specific cells, tissues or organs within the body [2]. Traditional carriers in DDs are biodegradable natural polymers, such as chitosan derivatives or polysaccharides, and synthetic polymers, such as hydrogels or dendrimers [3]. Nanomaterials have played a pivotal role in advancing drug delivery technology, expanding a wide spectrum of new nanocarriers, such as polymeric nanocapsules, liposomes vesicles and solid lipid nanoparticles [4]. Over the years, drug delivery methods have evolved to the use of a variety of inorganic materials, including silica and metallic oxide structures, and particularly those possessing significant porosity [5]. Recently, biological metal organic frameworks (bioMOFs), which are micro/mesoporous biocompatible structures, have been proposed as carriers for controlled drug delivery. BioMOFs are built with non-toxic metals and organic linkers of biological nature that can be either macromolecules (nucleobases, amino acids, polypeptides, proteins, porphyrins, etc.) or polytopic therapeutic biomolecules (curcumin, nicotinic acid, etc.) [6]. They offer further advantages over traditional drug carriers including compositional and structural diversity, framework flexibility and enhanced biocompatibility [7]. Unlike conventional DDs, which are often inert in regard of therapeutic value, bioMOFs can be constructed from building units possessing pharmaceutical activity [8,9].

The bioMOF CaSyr-1 has been recently developed in our laboratories with the aim of building DDs with full biocompatibility given by the framework composition defined as calcium cation (Ca^{2+}) nodes and phenolic syringate anion (Syr^{2-}) linkers [10]. Among described bioMOFs, CaSyr-1 shows outstanding textural properties, with extraordinary values of experimental specific surface area (*ca.* 1000–1100 m^2 g^{-1}) and micropore volume (*ca.* 0.30 cm^3 g^{-1}). These characteristics confer a remarkable cargo loading capacity to the material. The crystallographic description of CaSyr-1 indicates that the porosity arises from hexagonal and unidimensional channels with an effective diameter of 1.4 nm (Fig. 1). This wide pore diameter, together with the absence of narrow pore windows or entrances, would enable the encapsulation of a large variety of active ingredients of different molecular size, from small drug molecules to biomacromolecules. Indeed, CaSyr-1 has one of the largest pore diameter value described for microporous bioMOFs, close to that of the mesoporous counterparts [11]. Additionally, CaSyr-1 exhibits certain bioactivity itself, mainly given by the syringate with anti-oxidant and anti-inflammatory properties, among others [12]. Hence, when used as a drug reservoir, the simultaneous release of the framework components and loaded cargo can afford synergies to fight particular diseases or to reduce side effects. For instance, the triple bioactive release of calcium, syringate and ibuprofen from a CaSyr-1(ibuprofen) system has been recently described, expecting positive synergies for hypertensive patients [10]. CaSyr-1 framework is originated from weak coordination bonds stablished between the carboxylate O-donor groups in Syr^{2-} and Ca^{2+} cations, which can be easily replaced by coordinating water molecules. This characteristic gives the bioMOF a high potential for degradation in biological media [13]. Actually, moisture causes the fast transition of CaSyr-1 towards a non-porous crystalline phase. In some scenarios, as for hydrophobic ibuprofen, physiologically unstable bioMOFs can be contemplated as desirable delivery vehicles to increase drug bioavailability [10,14]. Nevertheless, in many other occasions, too fast degradation in moisture/water is an event that can compromise applicability during drug administration, as well as steadiness during formulation and storage.

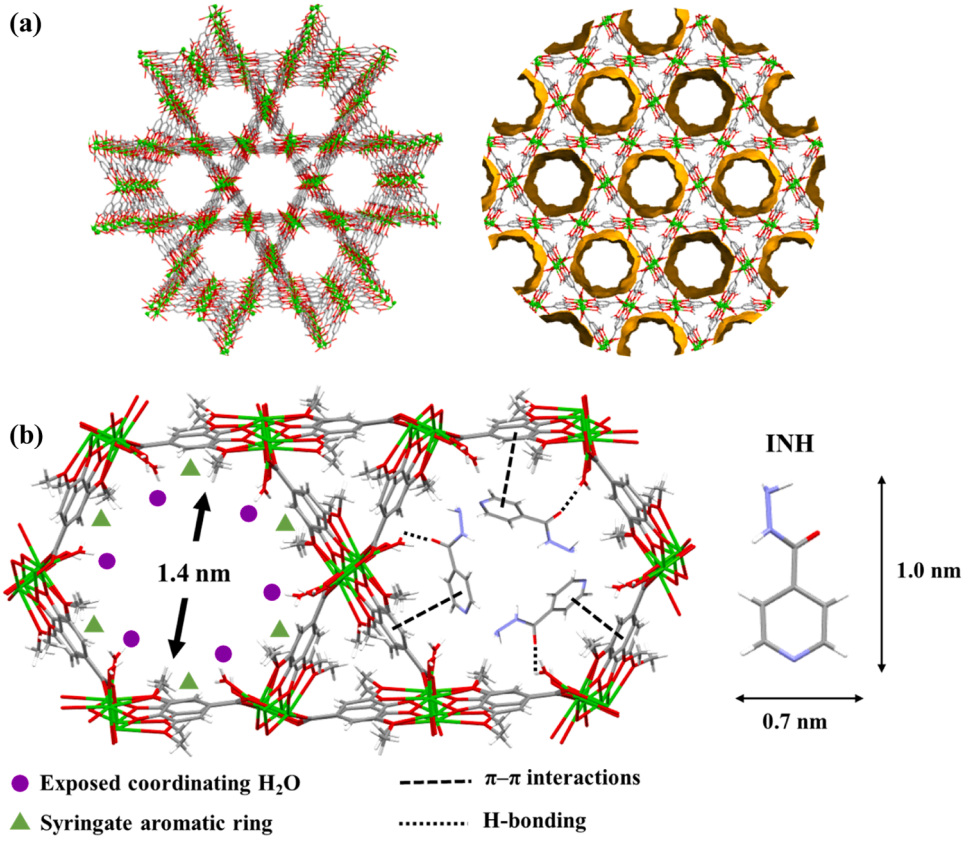

Fig. 1. Crystallographic structure of CaSyr-1: (a) hexagonal pores, and (b) projection of the pore wall functional groups interacting with loaded INH.

In this study, to impregnate, functionalize and modulate the dissolution behavior of CaSyr-1, the bioMOF is processed in supercritical CO_2 ($scCO_2$), a solvent widely used in the preparation of pharmaceutical formulations with important advantages [15], such as lack of toxicity and possibility of carrying out processes at near-ambient temperature [16]. The latter is important to avoid the thermal degradation of bioMOFs matrix, which can contain thermally labile organic linkers [17]. Moreover, the structure of MOFs can be sometimes altered by immersion in particular solvents, basically in those with high affinity for metals, leading to linker displacement and subsequent structural collapse or precipitation of a different phase. The use of $scCO_2$ is advantageous for the processing of MOFs, since this neutral solvent do not affect their crystalline structure [18]. $ScCO_2$ technology has been widely used to impregnate active agents and additives in polymeric and porous matrices [19,20]. This technology is used in this work to design a proper DDs based on CaSyr-1 nanoparticles (NPs), first to encapsulate a water-soluble drug (INH) into the pores of the bioMOF, and, second, to embed a water repellent agent (stearic acid, HS) on the outer surface of the NPs. The design of this particular DDs starts by using CaSyr-1 as a porous matrix for isoniazid (INH) loading, the reference antibiotic used in the first line treatment of mycobacterium tuberculosis infections, which is administered by oral or pulmonary route [21]. Continued treatment with INH is usually accompanied by serious side effects related to liver damage [22]. Conversely, many studies have indicated that syringic acid has hepatoprotective properties, and could mitigate the undesired hepatotoxic effects of isoniazid by the simultaneous delivery of INH/syringic acid co-crystallized products [23–25]. Moreover, net isoniazid suffers particle size redistribution during prolonged storage, reason why this drug should be preferably encapsulated in a matrix [26]. After $scCO_2$-mediated isoniazid impregnation, a biocompatible protective layer is deposited on the surface of CaSyr-1 NPs to attain a subtle balance between the necessary bioMOF degradability in biological media and sufficient stability to design proper administration routes for the loaded active agent. The research addresses kinetic factors affecting the bioMOF dissolution rate by the superficial incorporation of the bulky hydrophobic stearate (S), acting as a moist sensitivity modulator. HS is a saturated monobasic fatty acid with a C-18 chain that is widely used in the production of pharmaceutical tablets and capsules [27] and it is a lipid processed by $scCO_2$ to produce solid lipid nanoparticles [28]. The adjustment of the $scCO_2$ operating conditions allows to carry out both processes, impregnation and surface functionalization, by using the same technology. Additionally, the resulting material is further coated with polysorbate 60 (PS60), a neutral stearate-derived surfactant, to enhance the overall wettability of the system. The prepared drug nanocarrier involving CaSyr-1, S and PS60 displayed full biocompatibility, even at elevated concentrations, which is ascribed to the rational design and synthesis of the DDs, including only bio-based products and pharmaceutically approved solvents such as $scCO_2$ and ethanol.

2. Materials and procedure

2.1. Materials

The employed reactants for CaSyr-1 synthesis were syringic acid (H_2Syr 98 %, abcr) and calcium acetylacetonate ($Ca(acac)_2$ 98 %, abcr). The loaded active compound was INH (99 %, Sigma-Aldrich). The selected additives were HS (95 %, Merck) used as a modulator for hydrophobicity and PS60 (Sigma-Aldrich) used as a surfactant. The employed solvents for the synthesis of the material were absolute ethanol (EtOH, Scharlab), compressed CO_2 (99.95 wt%, Carburos Metálicos S.A.) and ethyl acetate (EtOAc, Scharlab).

2.2. Synthetic procedure

CaSyr-1 nanopowder was synthesized following a reported method [10]. In short, 238 mg of $Ca(acac)_2$ and 198 mg of H_2Syr were separately suspended and dissolved in 5 mL of EtOH, added to a vial and mixed by vortex agitation. After 30 min resting at room temperature, the precipitated CaSyr-1 NPs were recovered by centrifugation and washed thrice with EtOH. CaSyr-1 was activated at 393 K under vacuum (*ca.* 15 Pa) for 6 h to fully empty the pores from residual solvent.

The loading of CaSyr-1 with INH was carried out in a static mode under stirring (500 rpm) by using $scCO_2$ at 333 K and 20 MPa, lasting the run for *ca.* 60 h. For this, excess of INH (164 mg) was added to a small vial (together with a stir bar) and placed into a 100 mL high-pressure vessel (Thar Design) holding 150 mg of activated CaSyr-1 enclosed in a permeable cartridge of filter paper. The system was pressurized up to 20 MPa by using a Teledyne Isco 260D syringe pump and heated with resistances. After drug impregnation, the autoclave was depressurized at a relatively low rate in a two-step procedure (*ca.* 2–3 MPa min^{-1} in the range 20–9 MPa and *ca.* 0.5 MPa min^{-1} from 9 MPa to ambient), and then cooled down to room temperature to recover the cartridge enclosing the CaSyr-1(INH) product. In this set-up, matrix and solute were physically separated to avoid potential contamination of the formulation by undissolved solid drug. The exterior of the recovered cartridge was flushed with a jet of pressurized N_2 gas to eliminate any potential solid particles of INH deposited on the filter paper surface. Indeed, most of the INH excess remained in the vial, and only a very small amount of crystals was found precipitated on the high pressure vessel walls, the coldest area in the autoclave due to CO_2 Joule-Thomson effect during depressurization. From the recovered sample, drug loading or content are defined as the impregnated mass of drug divided by either the mass of pristine matrix ($wt_{INH}/wt_{CaSyr\text{-}1}$ x 100) or the mass of impregnated matrix ($wt_{INH}/wt_{(INH+CaSyr\text{-}1)}$ x 100).

The functionalization of CaSyr-1(INH) with stearic acid in $scCO_2$ was carried out in the same 100 mL high-pressure vessel containing a vial filled with 140 mg of stearic acid and a stirrer, and 120 mg of CaSyr-1 (INH) NPs wrapped in a cartridge of filter paper. The system was heated at 333 K and pressurized up to 15 MPa, while stirring at 500 rpm. These conditions were maintained for 20 h. Afterwards, the autoclave was depressurized to 6 MPa, pressurized again with fresh CO_2 to 15 MPa and depressurized to ambient pressure. This washing step was repeated two times under isothermal conditions to remove the excess of stearic acid. Finally, the autoclave was cooled down to recover the CaSyr-1 (INH)/S sample.

CaSyr-1(INH)/S was further coated with PS60. For that, 1000 mg of PS60 were placed into a vial and melted at 323 K. 120 mg of CaSyr-1 (INH)/S were then added and the mixture was soaked at 323 K for 2 h. The viscous suspension was diluted with a small amount (0.5 mL) of EtOAc, collected by vacuum filtration and washed with 1 mL of fresh EtOAc to eliminate the excess of PS60, thus recovering a powder of the end product CaSyr-1(INH)/S/PS60.

2.3. Characterization

2.3.1. Physicochemical and morphological properties

Proton nuclear magnetic resonance (^{1}H NMR, Bruker Avance NEO 300 MHz) was used to quantify the molar ratio of INH with respect to H_2Syr (see supplementary material for Figs. S1-S6) in the samples collected after impregnation (Fig. S1), surface functionalization (Fig. S2) and coating (Fig. S3). The analysis was carried out in dimethyl sulfoxide-d_6 (DMSO-d_6; 99.5 v% d_6, abcr), after digesting each sample in hydrofluoric acid (HF; 40 v% in water, Fluka). The INH signal at $\delta = 7.74$ ppm (Fig. S4) was integrated with respect to the H_2Syr signal at $\delta = 7.21$ ppm (Fig. S5), both signals corresponding to the integration of 2 H in the respective pristine organic molecules. In the functionalized sample (Fig. S2), the stearic acid signal at $\delta = 1.48$ ppm (Fig. S6) was also integrated with respect to the H_2Syr signal at $\delta = 7.21$ ppm (Fig. S5) to estimate the content of the fatty acid in the system. Powder X-ray diffraction (XRD, Siemens D5000) patterns were recorded for the different samples in the 2θ range 5–30°. Scanning (SEM, Quanta FEI 200

FEG-ESEM) and transmission (TEM, JEOL 1210) electron microscopes were utilized to evaluate the morphology and the size of the NPs. For the different samples, histograms of the particle size distribution were obtained by measuring > 200 discrete particles in images taken with TEM and using ImageJ program for analysis. Dynamic light scattering (DLS, Zetasizer Nano ZS Malvern Inst.) was employed to measure the dynamic size of CaSyr-1 and CaSyr-1(INH)/S/PS60 particles suspended in EtOH and H_2O, respectively. N_2 physisorption at 77 K (ASAP 2020 Micromeritics) was applied to estimate the porosity of the composites. Previous to the analysis, the samples were activated overnight at 393 K under vacuum. From the recorded N_2 adsorption/desorption isotherms, the micropore volume was determined by the t-plot method, while the mesopore specific surface area was calculated by applying the Brunauer-Emmet-Teller (BET) equation.

2.3.2. *In vitro biocompatibility test*

The biocompatibility of the nanocarriers CaSyr-1 and CaSyr-1/S/PS60 was tested on a human osteosarcoma cell line (MG63, ATCC CRL1427). Prior to testing, the samples were sterilized at 413 K for 5 hours under dry conditions. MG63 cells were cultured in MEM NEAA medium (Sigma Aldrich), supplemented with 10 wt% fetal bovine serum (FBS, Sigma), 1 wt% penicillin/streptomycin (Invitrogen), and 2 wt% L-glutamine (Invitrogen). Cells were maintained at 310 K with 5 v% CO_2 in a humidified chamber until confluence before the assays. Cells from passages 4–8 were used in all experiments. 200 μL of MG63 cells were seeded on transwell inserts (collagen coated, cut-off = 0.4 μm, diameter = 6.5 mm, Costar) at a density of 100,000 cells mL^{-1}. The inserts were incubated in a 48-well plate with 400 μL of culture medium at 310 K and 5 v% CO_2. After 24 hours, the medium in the inserts was replaced with fresh medium, and the medium in the well plate was replaced with serial dilutions of CaSyr-1 and CaSyr-1/S/PS60 in culture medium (starting at 25 mg mL). After another 24 hours, all media were replaced with culture medium without phenol red. Cell viability was assessed by adding Alamar Blue (AB, Invitrogen) at 10 v% and incubating the cells at 310 K for 4 hours. Viability was measured using a plate reader (Biotek Synergy HT spectrophotometer) with excitation at 590 nm and emission at 530 nm. The cell viability (%) was calculated using the following formula: 100 x (ODS-ODB)/(ODC-ODB), where ODS, ODB, and ODC represent the emitted fluorescence at 530 nm for the sample (S), blank (B, culture medium without cells), and control (C), respectively. Experiments were performed in triplicate for each sample, and data was expressed as mean values ± standard deviation.

2.3.3. *Release of bioactive compounds*

The release of the organic bioactive compounds, *i.e.*, syringic acid and INH, from the assembled DDs, CaSyr-1(INH)/S/PS60, and CaSyr-1(INH) for comparison, was studied in PBS at 310 K. The standard solutions and the studied aliquots were analyzed by high-performance liquid chromatography (HPLC, Shimadzu Prominence LC-20AD Liquid Chromatograph, equipped with a Kromaphase C18 column). The employed mobile phase was a mixture of methanol/water (MeOH/H_2O; 20/80 v/v), applied with 0.5 mL min^{-1} flow rate and 6.2 MPa. The recorded retention times for H_2Syr and INH were 5.0 and 7.5 min, respectively. For both components, the UV-Vis spectra was analyzed at λ = 266 nm. Prior to aliquot analysis, calibration curves were constructed from several standards. For analyte concentration measurements, a weighted amount of sample, 25 mg for CaSyr-1(INH) and 30 mg for CaSyr-1(INH)/S/PS60, was immersed in 25 mL of PBS (pH = 7.4) at 310 K. Flasks were immediately placed into an orbital shaker incubator at the same temperature with the oscillation mode fixed at 100 rpm. Aliquots of 0.5 mL were collected after specific periods. The aliquots were then diluted in 1 mL of mobile phase and passed through PTFE syringe filters (0.45 μm) before analysis. The content of the bioactive compound in each aliquot was estimated by extrapolating the experimental signal in the equation obtained from the calibration curve of each compound, and considering the dilution factors. Each experiment was performed in triplicate and the results were given as mean values ± standard deviation.

3. Results and discussions

3.1. *Synthesis and characterization*

The synthesis of the designed DDs involving CaSyr-1/INH/S/PS60 is carried out stepwise following the procedure schematized in Fig. 2. CaSyr-1 was obtained following a facile, fast and non-solvothermal synthesis by simply mixing the starting materials in EtOH at room temperature (Fig. 3(a)). SEM images indicated that the bioMOF precipitated as isometric particles of 50–100 nm diameter (Fig. 4(a)) with narrow size distribution determined by TEM (Fig. S7 in supplementary material). Although CaSyr-1 is stable for at least one month when stored under ambient conditions, this material is thermodynamically unstable in contact with water, solvent in which the NPs are instantaneously dissolved with the subsequent precipitation of a dense non-porous phase. The significant kinetic stability of CaSyr-1 under moisture (60 % relative humidity and 298 K) is taken as a benefit for making the bioMOF suitable for further processing, *e.g.*, for loading with an active agent. Nevertheless, for its reliable application in DDs, the kinetic stability in aqueous media must be enhanced. This aspect is addressed in this work by hydrophobizing the material. Both processes, drug impregnation and hydrophobization of CaSyr-1 NPs, are performed consecutively by using $scCO_2$ technology, a solvent widely used in the preparation of pharmaceutical products [29]. This technology is here used to encapsulate the drug inside the pores of the bioMOF and to embed the water repellent agent on the outer surface of the NPs.

INH was chosen as the active agent for CaSyr-1 impregnation. This choice was rigorously taken considering some physicochemical aspects of INH with respect to CaSyr-1, including the molecular size (1.0 ×0.7 nm, suitable for entering the 1.4 nm CaSyr-1 channels), the potential supramolecular interactions in the pores and the respective hepatotoxic and hepatoprotective properties. INH drug has been already impregnated in other MOFs of the iron trimesate family by using water as the carrier fluid [30,31]. However, due to the chemical instability of CaSyr-1 in water, $scCO_2$ is used in this work as a proper alternative solvent. Despite the highly polar character of INH, this drug presents some solubility in $scCO_2$, with reported values of 4–6 $\times 10^{-6}$ mole fraction at 15–20 MPa and 313 K [32]. In this fluid, the primary amino group contained in INH can react with CO_2 to produce insoluble carbamates through the formation of zwitterion intermediates [33]. The generation of these insoluble species is minimized at high operating temperatures, reason why the impregnation process in $scCO_2$ was carried out at 333 K, which would also enhance the intrinsic solubility of the drug by increasing its vapor pressure. Even so, the attained solubility values of INH in $scCO_2$ would be low, thus, long equilibrium times have been applied in the adsorptive impregnation process. Drug confinement by adsorptive impregnation inside porous materials has been defined to start with an adsorption process [34]. For materials with pore diameter larger than the solute size by a factor of 10–20, drug crystals can be formed, while for small pores, amorphous phases generally precipitate. In the studied pair CaSyr-1/INH, the pore size of the micrometric matrix just slightly exceeds the molecular diameter of the solute (1.4 nm *vs. ca.* 1 nm, respectively). With such a small pore diameter, solute precipitation inside the pores is not expected for neither crystalline nor amorphous phases. As defined by the IUPAC technical report on physisorption [35], solute confinement inside micrometric pores below 2 nm is better defined by micropore filling than by surface adsorption. Hence, the physical state of INH inside CaSyr-1 pores can be approximated to liquid, which, in regard of molecular order, is considered closer to amorphous solids. Actually, the process in this work can be defined as a molecular adsorptive impregnation, in which the formation of a drug solid phase is not envisaged [20]. Under the working static conditions, kinetics can be defined by either drug dissolution, or by its transport to

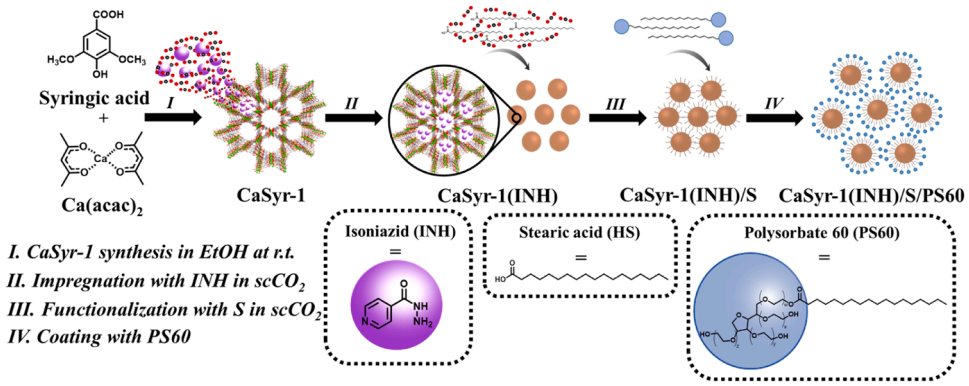

Fig. 2. Schematic representation of the synthetic protocol highlighting the consecutive main steps: precipitation of CaSyr-1 in EtOH, impregnation with INH for CaSyr-1(INH) in $scCO_2$, surface functionalization with S for CaSyr-1(INH)/S in $scCO_2$ and coating with PS60 for CaSyr-1(INH)/S/PS60.

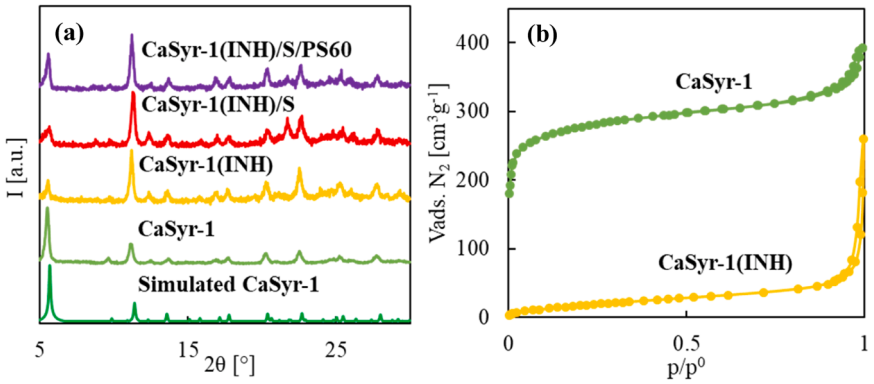

Fig. 3. Structural and textural characterization of the studied samples: (a) powder XRD patterns of samples CaSyr-1, CaSyr-1(INH), CaSyr-1(INH)/S and CaSyr-1(INH)/S/PS60 compared with the simulated phase, and (b) N_2 adsorption/desorption isotherms of samples CaSyr-1 and CaSyr-1(INH).

the adsorbent surface or diffusion/adsorption into the pores. Even for the slightly soluble INH, drug dissolution is likely not the rate-determining step in the used stirred autoclave [36]. Drug diffusion in the $scCO_2$ medium can be the rate limiting step at early stages, until the solution reach equilibrium. After that, intraparticle diffusion would determine the kinetics. The chemical composition of the bioMOF is the key parameter to ensure successful drug incorporation, since infused molecules must be stabilized at the interior of the channels by supramolecular interactions with the pore walls. For the INH/CaSyr-1 pair, the INH interactions include hydrogen bonding with the exposed coordinating waters and π–π interactions with the syringate aromatic rings (Fig. 1(b)). According to ^{1}H NMR quantitative analysis (Fig. S1), the recovered CaSyr-1(INH) sample contains 0.3 mol of INH per mol of CaSyr-1, which implies a mean drug content of 14.7 wt% (drug loading of 17.3 wt%), with a deviation of ± 2 %. For this sample, the XRD pattern displays all the peaks of CaSyr-1 (Fig. 3(a)), demonstrating, first, that the structure of the bioMOF was not damaged during $scCO_2$ treatment. Moreover, the main peaks of INH, expected at $2\theta = 9.25$ and 24.2°, are not present in the diffractogram. Overall, only some differences in the relative intensity of the peak at $2\theta = 5.7°$ could be spotted, which is ascribed to CaSyr-1 micropore filling, thus indicating that the active agent was molecularly impregnated inside the channels and the outer surface and not precipitated as crystals on the bulk. Likewise, SEM images show only CaSyr-1 NPs, free of the typical needles formed by INH recrystallization in $scCO_2$ (Fig. 4(b)). Comparing with the N_2 adsorption-desorption isotherm of pristine CaSyr-1, CaSyr-1(INH) experiences a complete drop of N_2 adsorption in the micropore region, which indicates that the bioMOF pores were blocked by incorporation of the active agent (Fig. 3(b)). CaSyr-1(INH) only exhibits some meso/-macroporosity originated by NPs aggregation, with a BET specific surface area of 70 $m^2\ g^{-1}$. Giving a geometrically predicted molar volume of 110 cm^3 for INH, 0.3 mol of this molecule would occupy *ca.* 33 cm^3. Before impregnation, the empty volume of pristine CaSyr-1 NPs was calculated from the N_2 physisorption data by using the t-method as 81 $cm^3\ mol^{-1}$. Hence, near 40 v% of the CaSyr-1 empty channels were loaded with INH molecules by using the $scCO_2$ impregnation method, which is considered as an extraordinary loading value for a poorly soluble drug in $scCO_2$ (in the order of 10^{-6} mole fraction).

CaSyr-1(INH) sample reveals similar instability in water than pristine CaSyr-1, which would trigger the instantaneous release of INH and the precipitation of CaSyr-2. Considering the physicochemical properties of CaSyr-1, it is reasoned that kinetically water-stable CaSyr-1(INH) NPs can be obtained by protecting the calcium coordination sphere on the NPs outer surface from water attack, for instance, by surface functionalization with a proper capping agent. Stearic acid, endowing a hydrophobic aliphatic tail and a carboxylic polar head with high affinity to calcium, was selected for this purpose. To configure the protective layer, consisting of stearate bonded to calcium on the NPs surface, CaSyr-1(INH) NPs were treated with a mixture of stearic acid and $scCO_2$ at 15 MPa and 333 K. Under these experimental conditions, the solubility of stearic acid is in the order of 1.1×10^{-3} mole fraction [37]. The process was carried out at a similar temperature than INH impregnation, but reducing the pressure from 20 to 15 MPa with a concomitant CO_2 density drop that is expected to minimize, if any, the loss of loaded INH by re-dissolution in the fluid phase. Actually, quantitative ^{1}H NMR analysis indicates a similar INH:CaSyr-1 molar ratio for both CaSyr-1(INH) and CaSyr-1(INH)/S samples (0.3:1, Fig. S2). The recorded XRD pattern for CaSyr-1(INH)/S is similar to that of CaSyr-1 (Fig. 3(a)), with an extra wide signal at $2\theta = 21$–22° attributed to the formation of calcium stearate on the NPs surface, likely together with some residual

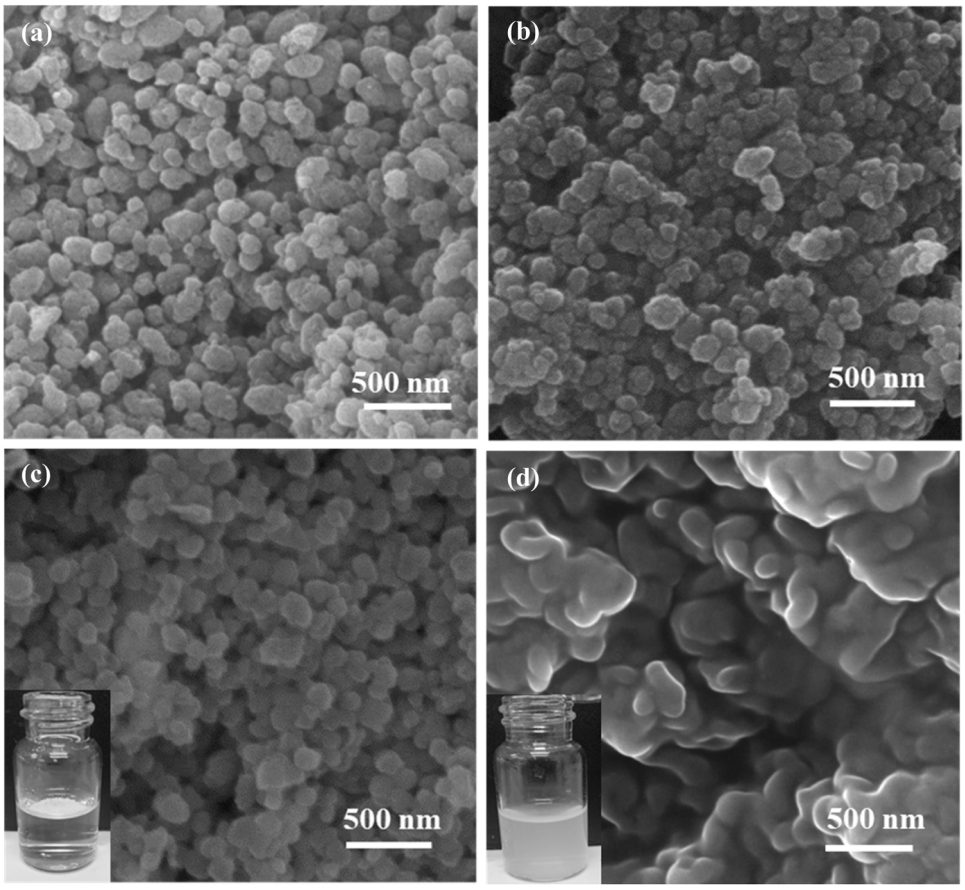

Fig. 4. SEM images of samples: (a) CaSyr-1, (b) CaSyr-1(INH), (c) CaSyr-1(INH)/S, and (d) CaSyr-1(INH)/S/PS60. The insets in the bottom-left corner for (c) and (d) correspond to the respective behavior of the samples in water.

stearic acid, both phases presenting intense diffraction peaks at these angles [38]. The presence of stearate did not generate noteworthy differences on the bulk appearance (Fig. 4(c)) and size (Fig. S8 in supplementary material) of CaSyr-1 NPs, although in TEM images the surface of the particles appear to be less smooth (Fig. S8), probably caused by the presence of disordered stearate chains in the external dominium. The specific amount of stearate in the composite was measured by ^{1}H NMR as 2 $\times 10^{-3}$ mol $g^{-1}_{Casyr\text{-}1}$ (Fig. S2). Considering the surface area occupied by one mole of stearate polar heads as *ca.* 4 $\times 10^8$ cm^2 mol^{-1} (the stearate head molecular diameter is estimated as 0.3 nm), the specific surface area that can be covered with the incorporated amount of stearate is *ca.* 80 m^2 g^{-1}. This area value is slightly higher than the experimental value found for the outer specific surface area of CaSyr-1 (INH), which was measured as 70 m^2 g^{-1}. Hence, total coverage with stearate carboxylate heads anchored on the outer surface of the NPs as a monolayer can be assumed, with only a small percentage of stearic acid in excess.

The obtained CaSyr-1(INH)/S NPs shows particularly high hydrophobicity and cannot be soaked in water, not even upon vigorous stirring (Fig. 4(c)_inlet). However, wettability is an indispensable parameter for DDs to achieve an effective travelling across body fluids and also, to enhance biocompatibility. In order to modulate the polarity of the external surface, CaSyr-1(INH)/S was further treated with PS60, a non-ionic surfactant derived from stearic acid widely used as an additive in pharmacy and food industry. Hence, strong hydrophobic interactions between the aliphatic domains of stearate and PS60 are envisaged. This process was carried out by using an almost solvent-free method, just by soaking CaSyr-1(INH)/S in fused PS60. According to XRD characterization, the composite structure was not modified by PS60 addition (Fig. 3(a)). Additionally, ^{1}H NMR analysis indicated that the molar ratio of INH:CaSyr-1 was preserved (Fig. S3). Although the morphology and size of CaSyr-1(INH)/S NPs was not modified (Fig. S9 in supplementary material), a thin film of amorphous PS60 can be observed embedding the nanocrystals (Fig. 4(d)). Regardless, according to DLS, the dynamic particle size distribution under suspension for the assembled DDs was in the order of 200–300 nm (Fig. S10 in supplementary material). By adding this second layer, the hydrophobic character of CaSyr-1(INH)/S was reverted and the resulting CaSyr-1(INH)/S/PS60 NPs were easily dispersed in water (Fig. 4(d)_inlet). The assembled stearate-based protective layers are expected to hinder the free diffusion of water molecules towards the CaSyr-1 framework, thus slowing down the release of the bioactive components.

3.2. Cytotoxicity

The toxicity of the assembled drug delivery system was tested to evaluate the suitability of the material for pharmaceutical applications. The assay was performed to estimate the IC_{50} of the matrix CaSyr-1/S/PS60, without the presence of impregnated INH, in order to avoid misleading results associated with drug toxicity. Data was compared to that obtained for pristine CaSyr-1 NPs. In the assay, samples were diluted to different concentrations and then immersed in MG63 cell culture. Remarkably, CaSyr-1/S/PS60 exhibited null toxicity at all the studied concentrations, even at 25 mg mL^{-1}, at which cell viability for pristine CaSyr-1 was negligible (Fig. 5(a)). The partial low toxicity of CaSyr-1 in the synthesized nanocarrier is not reflected in the reported results since the wt% ratio of CaSyr-1 in CaSyr-1/S/PS60 sample is much lower than in the pristine material. On the whole, these results indicate that the assembled protective layers on the outer surface of the bioMOF nanoparticles do not provide any additional toxicity to the system. This

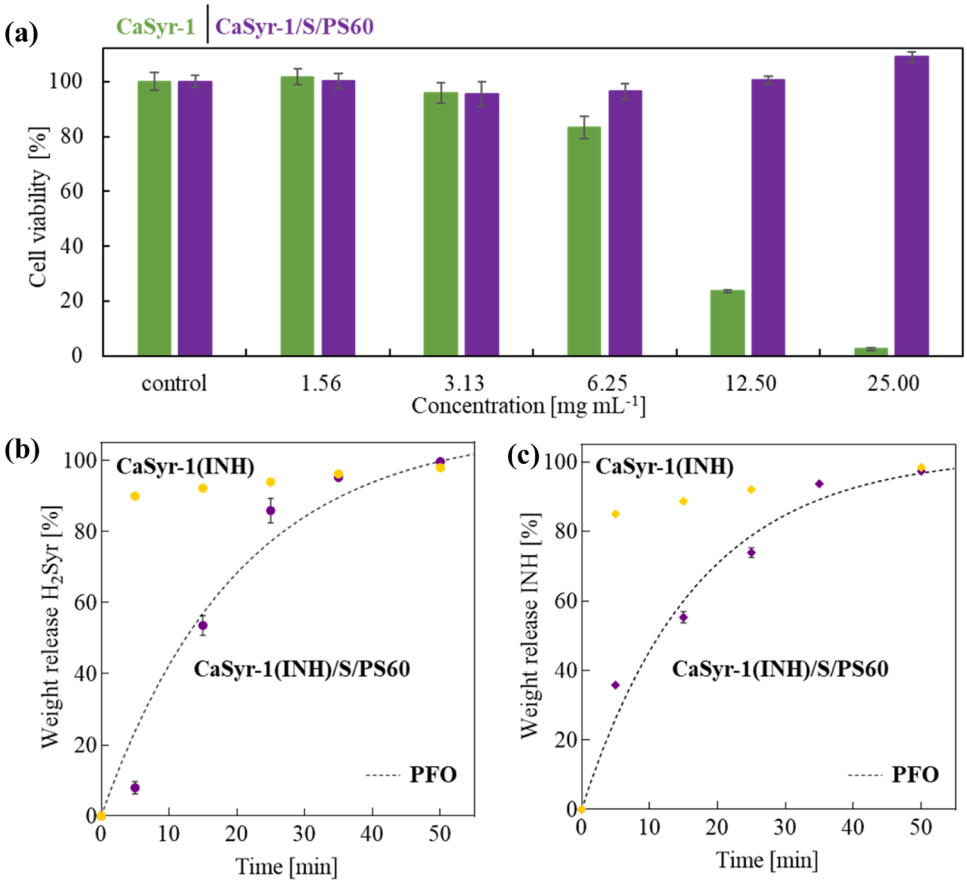

Fig. 5. *In vitro* tests: (a) cell viability of MG63 cell line in different concentrations of CaSyr-1 and CaSyr-1/S/PS60, and bioactive release of (b) H_2Syr and (c) INH from CaSyr-1(INH) and CaSyr-1(INH)/S/PS60 (the discontinuous line refers to the PFO fitting curve in CaSyr-1(INH)/S/PS60 sample).

unusual biocompatibility at high concentrations is the result of the intrinsic biocompatibility of the designed CaSyr-1/S/PS60 drug nanocarrier components, together with the use of green and non-toxic solvents for the assembly of the material.

3.3. Bioactive release

To study the multicomponent drug release, impregnated CaSyr-1(INH) and CaSyr-1(INH)/S/PS60 samples were immersed in an aqueous solution of PBS (pH = 7.4) under 100 rpm (oscillation) at 310 K. The concentration of H_2Syr and INH in the liquid phase was measured by HPLC at different times. For the CaSyr-1(INH) sample, both Syr^{2-} and INH were completely released from the framework immediately upon immersion into the physiological medium (Fig. 5(b,c)). The fast dissolution and release is attributed to the polar character of the bioMOF, which fosters the rapid penetration of water molecules within the pores of CaSyr-1 and simultaneous bioMOF dissolution and INH delivery. Instead, for the CaSyr-1(INH)/S/PS60 sample the complete release of the components was delayed up to *ca.* 30 min (Fig. 5(b,c)). In this sample, the release profiles of INH and H_2Syr followed similar patterns, indicating that again INH release is driven by CaSyr-1 dissolution. Both profiles can be fitted to the pseudo-first order (PFO) kinetic model, which is representative of biodegradable nanocarriers [39].

It has been described that the serious side effects of INH in the liver can be reduced by administering the drug through the pulmonary instead of the oral route [40]. Concurrently, the specific potential for aerosol delivery of bioMOFs for pulmonary therapies has recently appeared in the literature [41]. With appropriately designed inhalation devices such as pressurized metered-dose inhaler, dry powder inhalers and nebulizers, the CaSyr-1(INH)/S/PS60 ultrafine nanoparticles would efficiently penetrate deep lung tissues and deposit in the airway by Brownian motion, entering the alveolar area where tubercular bacilli reside [42,43]. The designed DDs would easily dissolve in lung fluids, with similar composition to PBS but also consisting of complexing anions and functional groups known to chelate metals. Unlike the described behavior of CaSyr-1 in water, the non-porous phase does not precipitate in body fluids since the formation of calcium phosphate salts prevents the arrangement of the coordination polymer. Hence, upon framework dissolution, the syringate anion would be free to accomplish its hepatoprotective function.

4. Conclusions

The $scCO_2$ technology is used to obtain a novel DDs by loading the anti-tubercular drug INH into CaSyr-1 nanocarrier to afford CaSyr-1(INH). Moreover, the same technology is used to post-synthetically encapsulate CaSyr-1(INH) NPs with a protective matrix (S/PS60), thus extending the applicability of the system towards administration in aqueous media. $ScCO_2$ is used as a solvent in a stepwise process, in which the solute (either isoniazid or stearic acid) solubility is modulated by varying the system pressure in the range of 15–20 MPa. Loadings of *ca.* 14.7 wt% of INH into de pores of CaSyr-1 are thus obtained, while the NPs could be coated with a near monolayer of stearic acid. From the final product CaSyr-1(INH)/S/PS60, the release of the drug in a body simulated fluid occurs in a period of *ca.* 30 min, time enough for the CaSyr-1 nanoparticles to reach the alveolar lung region when pulmonary administration is followed. The advantages of the designed DDs include expected synergistic therapeutic effects between the loaded INH drug and the syringate component in CaSyr-1, with hepatotoxic and hepatoprotective characteristics, respectively. Finally, it is shown that the

inherent biocompatibility of CaSyr-1/S/PS60 components as well as the followed green synthesis and processing of the material results in a DDs with null cytotoxicity.

CRediT authorship contribution statement

María Rosa Aguilar: Validation, Resources, Project administration, Funding acquisition. **Luis García-Fernández:** Validation, Resources, Methodology. **Albert Rosado:** Writing – original draft, Software, Methodology, Investigation, Data curation, Conceptualization. **Concepcion Domingo:** Writing – review & editing, Writing – original draft, Validation, Supervision, Resources, Project administration, Investigation, Funding acquisition. **José A. Ayllón:** Writing – review & editing, Validation, Supervision, Project administration, Funding acquisition. **Ana M. López-Periago:** Writing – review & editing, Validation, Supervision, Resources, Project administration, Funding acquisition. **Rosa Ana Ramírez:** Validation, Software, Methodology.

Declaration of Competing Interest

The authors declare that they have no known competing financial interests or personal relationships that could have appeared to influence the work reported in this paper.

Acknowledgements

This work was supported by the Spanish Ministry of Science and Innovation MICINN through the Severo Ochoa Program for Centers of Excellence (CEX2023–001263-S), by the Spanish National Plan of Research with projects PID2020–115631GB-I00 and PID2020–114086RB-100, and by CIBER (Spain) - Consorcio Centro de Investigación Biomédica en Red (Ref. CB06/01/0013), Instituto de Salud Carlos III. This research work was performed in the framework of the Nanomedicine CSIC HUB (Ref. 202180E048). A.R. acknowledges the financial support of FPI 2019 grant. This work has been performed in the framework of the doctoral program “Chemistry” of the Universitat Autònoma de Barcelona by A. R.

Appendix A. Supplementary data

Supplementary material: ^{1}H NMR composition analysis and particle size characterization, including TEM and DLS.

Appendix A. Supporting information

Supplementary data associated with this article can be found in the online version at doi:10.1016/j.supflu.2024.106452.

Data Availability

Data will be made available on request.

References

[1] H. Park, A. Otte, K. Park, Evolution of drug delivery systems: from 1950 to 2020 and beyond, J. Control. Release 342 (2022) 53–56.
[2] A.M. Vargason, A.C. Anselmo, S. Mitragotri, The evolution of commercial drug delivery technologies, Nat. Biomed. Eng. 5 (2021) 951–967.
[3] Y.K. Sung, S.W. Kim, Recent advances in polymeric drug delivery systems, Biomater. Res. 24 (2020) 12.
[4] V.J. Lingayat, N.S. Zarekar, R.S. Shendge, Solid lipid nanoparticles: a review, Nanosci. Nanotech. Res. 4 (2017) 67–72.
[5] J. Gao, J.M. Karp, R. Langer, The future of drug delivery, Chem. Mater. 35 (2023) 359–363.
[6] E. Binaeian, H. Nabipour, S. Ahmadi, S. Rohani, The green synthesis and applications of biological metal–organic frameworks for targeted drug delivery and tumor treatments, J. Mater. Chem. B 11 (2023) 11426–11459.
[7] H.-S. Wang, Y.-H. Wang, Y. Ding, Development of biological metal–organic frameworks designed for biomedical applications: from bio-sensing/bio-imaging to disease treatment, Nanoscale Adv. 2 (2020) 3788–3797.
[8] S. He, L. Wu, X. Li, H. Sun, T. Xiong, J. Liu, C. Huang, H. Xu, H. Sun, W. Chen, R. Gref, J. Zhan, Metal-organic frameworks for advanced drug delivery, Acta Pharm. Sin. B 11 (2021) 2362–2395.
[9] D. Lv, W. Nong, Y. Guan, Edible ligand-metal–organic frameworks: synthesis, structures, properties and applications, Coord. Chem. Rev. 450 (2022) 214–234.
[10] A. Rosado, O. Vallcorba, B. Vázquez-Lasa, L. García-Fernández, R.A. Ramírez-Jiménez, M.R. Aguilar, A.M. López-Periago, C. Domingo, J.A. Ayllón, Facile, Fast and green synthesis of a highly porous calcium-syringate BioMOF with intriguing triple bioactivity, Inorg. Chem. Front. 10 (2023) 2165–2173.
[11] K. Wang, D. Feng, T.F. Liu, J. Su, S. Yuan, Y.P. Chen, M. Bosch, X. Zou, H.C. Zhou, A series of highly stable mesoporous metalloporphyrin Fe-MOFs, J. Am. Chem. Soc. 136 (2014) 13983–13986.
[12] C. Srinivasulu, M. Ramgopal, G. Ramanjaneyulu, C.M. Anuradha, C. Suresh Kumar, Syringic acid (SA) – A review of its occurrence, biosynthesis, pharmacological and industrial importance, Biomed. Pharmacother. 108 (2018) 547–557.
[13] S. Yuan, L. Feng, K. Wang, J. Pang, M. Bosch, C. Lollar, Y. Sun, J. Qin, X. Yang, P. Zhang, Q. Wang, L. Zou, Y. Zhang, L. Zhang, Y. Fang, J. Li, H.-C. Zhou, Stable metal–organic frameworks: design, synthesis, and applications, Adv. Mater. 30 (2018) 1704303.
[14] K. Suresh, A.J. Matzge, Enhanced drug delivery by dissolution of amorphous drug encapsulated in a water unstable metal-organic framework (MOF), Angew. Chem. Int. Ed. 58 (2019) 16790–16794.
[15] A. Martín, M.J. Cocero, Micronization processes with supercritical fluids: fundamentals and mechanisms, Adv. Drug Deliv. Rev. 60 (2008) 339–350.
[16] T. Athamneh, A. Amin, E. Benke, R. Ambrus, C.S. Leopold, P. Gurikov, I. Smirnova, Alginate and hybrid alginate-hyaluronic acid aerogel microspheres as potential carrier for pulmonary drug delivery, J. Supercrit. Fluids 150 (2019) 49–55.
[17] M. Kubovics, S. Rojas, A.M. Lopez, J. Fraile, P. Horcajada, C. Domingo, Fully supercritical CO_2 preparation of a nanostructured MOF composite with application in cutaneous drug delivery, J. Supercrit. Fluids 178 (2021) 105379.
[18] K. Matsuyama, Supercritical fluid processing for metal–organic frameworks, porous coordination polymers, and covalent organic frameworks, J. Supercrit. Fluids 134 (2018) 197–203.
[19] N.D. Machado, J.E. Mosquera, R.E. Martini, M.L. Goñi, N.A. Gañán, Supercritical CO_2-assisted impregnation/deposition of polymeric materials with pharmaceutical, nutraceutical, and biomedical applications: A review (2015–2021), J. Supercrit. Fluids 191 (2022) 105763.
[20] A.M. López-Periago, C. Domingo, Features of supercritical CO_2 in the delicate world of the nanopores, J. Supercrit. Fluids 134 (2018) 204–213.
[21] I. Sibum, P. Hagedoorn, H.W. Frijlink, F. Grasmeijer, Characterization and formulation of isoniazid for high-dose dry powder inhalation, Pharmaceutics 11 (2019) 233.
[22] I. Metushi, J. Uetrecht, E. Phillips, Mechanism of isoniazid-induced hepatotoxicity: then and now, Br. J. Clin. Pharmacol. 81 (2016) 1030–1036.
[23] N.V. Bhilare, S.S. Dhaneshwar1, K.R. Mahadik, Phenolic acid-tethered isoniazid for abrogation of drug-induced hepatotoxicity: design, synthesis, kinetics and pharmacological evaluation, Drug Deliv. Transl. Res. 8 (2018) 770–779.
[24] B. Yadav, A. Gunnam, R. Thipparaboina, A.K. Nangia, N.R. Shastri, Hepatoprotective cocrystals of isoniazid: synthesis, solid state characterization, and hepatotoxicity studies, Cryst. Growth Des. 19 (2019) 5161–5172.
[25] F. Liu, F.B. Jiang, Y.T. Li, R.M. Liu, Z.Y. Wu, C.W. Yan, Cocrystallization with syringic acid presents a new opportunity for effectively reducing the hepatotoxicity of isoniazid, Drug Dev. Ind. Pharm. 46 (2020) 988–995.
[26] A. Roda, F. Santos, A.A. Matias, A. Paiva, A.R.C. Duarte, Design and processing of drug delivery formulations of therapeutic deep eutectic systems for tuberculosis, J. Supercrit. Fluids 161 (2020) 104826.
[27] L.A. Felton, S.C. Porter, An update on pharmaceutical film coating for drug delivery, Expert Opin. Drug Deliv. 10 (2013) 421–435.
[28] P. Trucilloa, R. Campardelli, Production of solid lipid nanoparticles with a supercritical fluid assisted process, J. Supercrit. Fluids 143 (2019) 16–23.
[29] Crystalline curcumin bioMOF obtained by precipitation in supercritical CO_2 and structural determination by electron diffraction tomography, N. Portolés-Gil, A. Lanza, N. Aliaga-Alcalde, J.A. Ayllón, M. Gemmi, E. Mugnaioli, A.M. López-Periago, C. Domingo, ACS Sustainable Chem. Eng. 6 (2018) 12309–12319.
[30] C. Fernández-Paz, E. Fernández-Paz, P. Salcedo-Abraira, S. Rojas, S. Barrios-Esteban, N. Csaba, P. Horcajada, C. Remuñán-López, Microencapsulated isoniazid-loaded metal–organic frameworks for pulmonary administration of antituberculosis, Drugs, Molecules 26 (2021) 6408.
[31] G. Wyszogrodzka-Gaweł, P. Dorozynski, S. Giovagnoli, W. Strzempek, E. Pesta, W. P. Weglarz, B. Gil, E. Menaszek, P. Kulinowski, An inhalable theranostic system for local tuberculosis treatment containing an isoniazid loaded metal organic framework Fe-MIL-101-NH_2 - from raw MOF to drug delivery system, Pharmaceutics 11 (2019) 687.
[32] R. Heryanto, E.C. Abdullah, M. Hasan, Solubility of isoniazid in supercritical carbon dioxide, J. Chem. Eng. Data 55 (2010) 2306–2309.
[33] Z.J. Dijkstra, A.R. Doornbos, H. Weyten, J.M. Ernsting, C.J. Elsevier, J.T. F. Keurentjes, Formation of carbamic acid in organic solvents and in supercritical carbon dioxide, J. Supercrit. Fluids 41 (2007) 109–114.
[34] P. Gurikov, I. Smirnova, Amorphization of drugs by adsorptive precipitation from supercritical solutions: a review, J. Supercrit. Fluids 132 (2018) 105–125.
[35] M. Thommes, K. Kaneko, A.V. Neimark, J.P. Olivier, F. Rodriguez-Reinoso, J. Rouquerol, K.S.W. Sing, Physisorption of gases, with special reference to the

evaluation of surface area and pore size distribution (IUPAC technical report), Pure Appl. Chem. 87 (2015) 1051–1069.
[36] G. Caputo, M. Scognamiglio, I. De Marco, Nimesulide adsorbed on silica aerogel using supercritical carbon dioxide, Chem. Eng. Res. Des. 90 (2012) 1082–1089.
[37] P. Maheshwar, Z.L. Nikolov, T.M. White, R. Hartel, Solubility of fatty acids in supercritical carbon dioxide, JAOCS 69 (1992) 1069–1076.
[38] M. Gonen, S. Ozturk, D. Balkose, S. Okur, S. Ulku, Preparation and characterization of calcium stearate powders and films prepared by precipitation and Langmuir-Blodgett techniques, Ind. Eng. Chem. Res. 49 (2010) 1732–1736.
[39] Y. Fu, W.J. Kao, Drug release kinetics and transport mechanisms of non-degradable and degradable polymeric delivery systems, Expert Opin. Drug Deliv. 7 (2010) 429–444.
[40] A. Misra, A.J. Hickey, C. Rossi, G. Borchard, H. Terada, K. Makino, P.B. Fourie, P. Colombo, Inhaled drug therapy for treatment of tuberculosis, Tuberculosis 91 (2011) 71–81.
[41] I.E. Stewart, I. Luz, N.P. Mortensen, Consideration of metal organic frameworks for respiratory delivery, KONA Powder Part. J. 38 (2021) 136–154.
[42] J.C. Sung, B.L. Pulliam, D.A. Edwards, Nanoparticles for drug delivery to the lungs, Trends Biotechnol. 25 (12) (2007) 563–570.
[43] S. He, J. Gui, K. Xiong, M. Chen, H. Gao, Y. Fu, A roadmap to pulmonary delivery strategies for the treatment of infectious lung diseases, J. Nanobiotech. 20 (2022) 101.